공학석사 학위논문

Fine tumor evaluation within the metastatic rabbit lymph nodes using the ultrasound contrast agent

초음파 조영제를 이용한 토끼 종양의 전이 림프절 평가에 관한 연구

2016 년 8 월

서울대학교 대학원

융합과학부 나노융합전공

이현재

Fine tumor evaluation within the metastatic rabbit lymph nodes using the ultrasound contrast agent

지도교수 이 학 종

이 논문을 공학석사 학위논문으로 제출함
2016 년 8 월

서울대학교 대학원
융합과학부 나노융합전공
이 현 재

이현재의 공학석사 학위논문을 인준함
2016 년 8 월

위 원 장 _____ 김영훈 (인)

부위원장 _____ 이학종 (인)

위 원 _____ 박원철 (인)

Abstract

Fine tumor evaluation within the metastatic rabbit lymph nodes using the ultrasound contrast agent

Hyun Jae Lee

Programs in Nano Science and Technology

Department of Transdisciplinary Studies

Seoul National University

This study was conducted with the aim of establishing complicated metastatic tumor rabbit models, see how ultrasound contrast agent is imaged inside the metastatic lymph nodes (LN) of the induced tumor rabbit models, and to find out the threshold minimum and maximum sizes of tumors that contrast agent could distinguish. 11 tumor rabbit models were used in total, and three groups were divided based on the number of subculture days. Among every

group, sizes of the normal LN and the metastatic LN were similar, but all of metastatic LN were significantly larger than those of the normal lymph nodes. Appearances of the induced tumors within the LN however, were notably different, and the acquired ultrasound images showed the possibility of spotting precise areas of tumors even when tumors were partially induced, when the contrast agent was injected. In the future, based on these established animal models, various ultrasound experiments using Nano-sized contrast agents and comparative pathology evaluation research would be carried out.

Keywords: ultrasound contrast agent, metastatic lymph node, rabbit, tumor

Student Number: 2014-24881

Table of Contents

List of Figures and Tables

1. Introduction

Once malignant, metastatic cells spread into the LNs located outside the dissected LN, it becomes increasingly hard to cure cancer completely, via current medical therapies, which in turn greatly increases the risks of mortality [1]. Hence to achieve good cancer treatment outcomes, taking precautions to prevent metastasis to LN is very important, and to do that, early yet accurate diagnosis is the key. Among several methods of cancer diagnosis, sentinel lymph node (SLN) detection has received much attentions recently [2]. Pathological status of SNL often provides valuable information for doctors, prior to operations, to decide on patients' treatment plans and surgical procedures. Hence, SLN detection is considered to be very important, especially in the case of superficial tumor treatment that has been originated in the breast or skin [3]. Accurate metastases detection within

the lymph node is vital for staging purposes [4] because a lot of monograms could underestimate the true risk of nodal metastasis [5],[6]. Detecting lymph node metastases is difficult via imaging modality, and several imaging techniques were used to map the lymphatic drainages, such as inside the prostate and PCa, but until nowadays, no reliable imaging modality is still available [4]. There have been promising attempts to utilize near infrared (NIR) fluorescence imaging for imaging of SLNs in vivo, but the near infrared detection is normally limited to the depth of less than 2cm, which hinders its capacity for imaging deeper lymph nodes [7]. Significant improvements on three dimensional imaging techniques in the past years have been achieved, namely magnetic resonance imaging (MRI) and computer tomography (CT), but certain notable limitations exist, such as lacking sensitivity for the metastases detections smaller than 1 cm in size [8], which are

the most prevalent types of metastases that occurs in contemporary series [9],[10]. These are referred to as micro metastasis, which is a stage of metastasis when the secondary tumors are too small to be clinically detected. Poor acoustic windows [3] is another important limiting factor, which hinders them to be applied in certain clinical practices. Furthermore, utilizing hybrid radio colloid, or single-photon emission CT/CT (SPECT/CT) specific radioactive/fluorescent imaging agents for the sentinel node lymphoscintigraphy result in low cancer specificity [11],[12]. Superparamagnetic Iron oxide nanoparticles (SPIONs) enhanced MRI showed promising preclinical and clinical results [13],[14],[15],[16] but it is yet to be granted Food and Drug Administration approval in the USA, and it is not very suitable for intraoperative imaging since intraoperative MRI scanners are very expensive with large footprints which prevent them to be

widely available around the globe [8]. Application of ultrasound contrast agent has proven to be effective in overcoming these limitations [3]. Rapid yet safe diagnosis is possible using the ultrasound contrast agent. Hence, study has been carried out to see how the SonoVue, a commercially available ultrasound contrast agent that has been used in the Netherlands since 2001 [3], is imaged inside the metastatic lymph nodes of VX_2 tumor rabbit models as well as to find out the threshold minimum and maximum tumor sizes it could distinguish.

2.Background

2.1 Medical Ultrasound

Medical ultrasound is a diagnostic imaging technique that uses the ultrasound. It is noninvasive method to see the internal body structures such as muscles, joints, tendons, and internal organs. Ultrasound is part of sound waves with frequencies much higher than those of human audible ranges (>20,000Hz). Ultrasonic images are formed when probe sends pulses of ultrasound into the designated tissues or other organs. When the sound waves encounters a material that has different density, some of the sound wave is reflected back to the probe and it is received and detected as an echo signal. Travel time of echo signal to the probe is used to measure the depth of the tissue that is interfacing which causes the echo. The greater the differences, between the acoustic impedances, the bigger the echo signal. Then the sound waves echoes off and since different parts of tissues have different depths, varying degree of echoes are reflected off. Those bounced echoes are

recorded and displayed as an image. The most well-known type of image that is produced is the B-mode image, which shows the acoustic impedance of two dimensional cross section of the tissue. Ultrasounds have many advantages compared to other imaging modalities. It allows real time diagnosis, portable, does not use harmful ionizing radiation, relatively inexpensive to run and shows the structure of organs. Some disadvantages include inability to penetrate bone, performance is very bad when there is a gas existing between the transducer and the tissue of interest, due to large differences in acoustic impedance, largely operator dependent, and there is no scout image as there are with CT and MRI. However, most importantly, ultrasound is harmless according to World Health Organizations technical report series 875 (1998).

2.2 Ultrasound Contrast Imaging

Ultrasound contrast imaging, also known as contrast ultrasonography utilizes a contrast medium that is formed by microbubbles that encapsulate gases [17], which in turn enhances echogenicity of blood. This was first discovered by Dr Raymond Gramiak in 1968 and he named this concept ‘contrast-enhanced ultrasound [18]. Gas encapsulated microbubbles is intravenously administered in patient blood stream during the ultrasonography examination. If the microbubbles are too big, it cannot extravagate to the interstitial fluid, which makes it an ideal contrast agent for imaging micro vascularization for diagnostic purposes since the contrast media is totally intravascular. Ultrasonography could be used for the detection of hyper vascular metastatic tumor which shows a contrast uptake much quicker than the healthy biological tissues surrounding the tumor [19]. Ultrasonography could also be applied in quantitative perfusion [20] which is the relative measurement of blood flow [21] which allows identification of early patient’s response to an anti-cancerous drug treatment [22]. This

allows the clinicians to determine the best oncological therapeutic options [23]. Dr Nicolas Rognin in 2010 devised the method of parametric imaging of vascular signatures [24, 25]. This is known as a cancer aided diagnostic tool which facilitate the characterization of a suspicious tumor, which could be either benign or malignant, in an organ. This works based on medical computational science[26, 27] to analyze the time sequence of ultrasound contrast images as well as the digital video that has been recorded in real time during the examination.

For each pixel of tumor, two consecutive signal processing steps are applied. With respect to healthy tissues around the tumor, automatic classification of the vascular signature allocated to the unique parameter. Green indicates contrast uptake higher than that of healthy tissues and shows hyper-enhancement. Blue indicates contrast uptake lower than that of healthy tissues and show hypo-enhancement. Red indicates contrast uptake before the healthy tissue and shows fast hyper-enhancement. And lastly yellow indicates contrast uptake after the healthy tissue, and indicates fast

hypo-enhancement. Once all of signal processing is completed, the computer monitor shows the color spatial map of the parameter, which shows all of vascular information of the tumor in a parametric image [28]. Predominant colorization of the tumor has useful indications. Red indicates a suspicion of malignancy that has high risk of cancer and in this case, clinicians generally carry out biopsy to confirm the diagnosis result, or CT scan for validating the result. Yellow or green indicates the high possibility of benignity of the tumor. Biopsy is invasive and risky to carry out on benign tumors as well as the X-ray radiating CT scans, so advances in medical ultrasonography has many advantages. The parametric imaging of vascular signatures method has been proven to be effective in characterizing tumors in the liver [29], and in the cancer screening field, this could be applicable in other organs such as prostate or breast [30].

2.3 Ultrasound Contrast agent

Most commonly used ultrasound contrast agent is made up of gas filled microbubbles that are generally administered intravenously to the circulation system. Microbubbles have high degree of echogenicity, which means it has an ability to reflect ultrasound waves. The fact that great difference in echogenicity exists between the gas core of the microbubbles and the soft tissue within the body makes microbubble an ideal agent to carry out ultrasonic imaging since microbubble contrast agents enhances the ultrasound reflection of the ultrasound waves that produces an increased contrast sonogram due to high echogenicity differences. Applications include blood perfusion of organs and measuring blood flow rate etc. There are many types of microbubbles that differ in their shell composition and gas composition. Different types are made according to specific targets or needs. Regardless of the shell or gas composition, microbubble size overall is quite uniform, within the range of 1~4 micrometers in diameter. These are smaller than

the sizes of red blood cells, which means microbubbles could flow easily through the body blood circulations. The most common types of shell materials are lipid, polymers, albumins or galactose[31]. The type of shell material used is an important factor in determining how easily the immune system could take in the microbubble. The more hydrophilic material, the bigger tendency it could be taken up more easily, which in turn reduces the residence time in the blood circulation. This means less amount of time is available for the actual contrast imaging. The material also has significant effects on the mechanical strength of the microbubbles. The higher the elasticity, the more acoustic energy it could withstand before it bursts. The gas core is the most important part of the microbubble since it determines the echogenicity of the microbubble, and it could be composed of various gases such as perfluorocarbon, nitrogen or air [31]. When ultrasound is applied, ultrasonic frequency field causes gas to compress and oscillate to reflect the echo characteristics, and generate one of a kind sonogram. Heavy gases, such as

perfluorocarbon, are less water soluble, which means they are more likely to stay within the microbubble (less leak) which means less microbubble dissolution is likely to happen [32]. This means microbubbles with heavy gases generally last longer in the body circulation.

3. Methods

For the study, 11 tumor rabbit models were used. Type of tumor cell lines that are used in rabbit models are limited, and most widely used variety VX2 carcinoma, has been utilized. VX2 carcinoma were injected just below the right hind limb of New Zealand white rabbits subcutaneously to induce the popliteal lymph node metastasis, and let tumor to grow for two weeks. Rabbits were anaesthetized using isoflurane. Rabbits were supplied from one provider and they were all in between 2.0~2.5kg in weight. VX2 carcinoma subculture process is unique in nature since it is carried out in the form of in-vivo, rather than in-vitro generally. First, fresh tumor tissues without the signs of necrosis were extracted and collected. Then the collected tumor tissues were finely grinded and injected to other rabbits for inducing tumor. One whole subculture cycle should not exceed a month, from injection to tumor formation and testing. The only type of commercial ultrasound contrast agent that was used during the whole research was SonoVue (Bracco, Italy).

4. Results

11 tumor rabbits were divided into three groups, and the sizes of both metastatic and normal lymph nodes were measured.

Group	Rabbit Number	Days after Subculture	Metastatic LN size/cm	Normal LN size/cm
A	1	23	1.8	0.9
	2	23	2.5	0.6
B	3	19	1.7	0.8
	4	19	1.5	0.7
	5	19	1.8	0.9
	6	19	1.7	0.9
	7	19	1.9	0.6
C	8	14	1.5	0.7
	9	14	1.7	0.8
	10	14	1.4	0.7
	11	14	1.5	0.7

Table 1. Size comparison between the metastatic lymph nodes and the normal lymph nodes.

Using the ultrasound probe, popliteal lymph node has been spotted. After confirming the presence of popliteal lymph node, ultrasound contrast agent was injected and the ultrasound image was acquired after 1 minute of gentle massage.

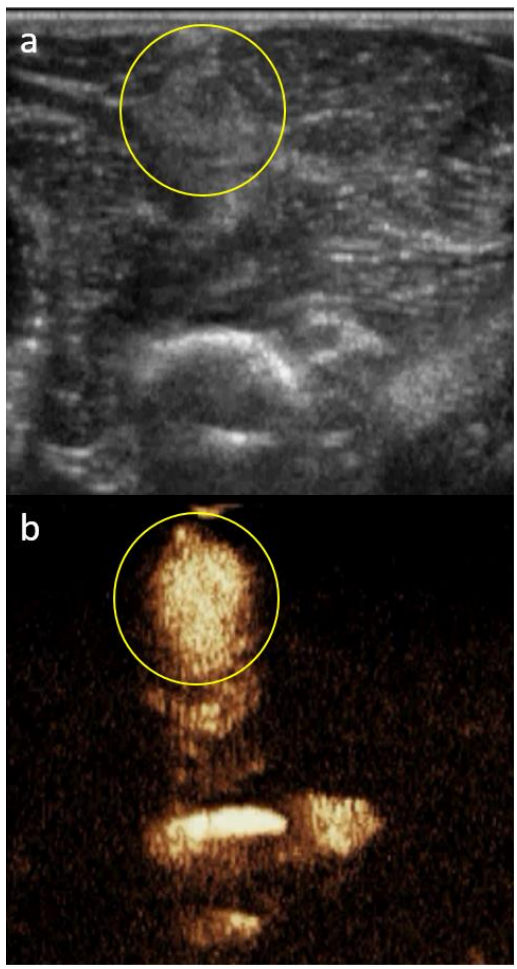

Figure 1. *a) Acquired ultrasound image showing the presence of popliteal lymph node*

b) Acquired ultrasound image after injecting SonoVue ultrasound contrast agent.

Actual photos of the metastatic lymph nodes as well as the normal lymph nodes are shown. On the dissected images, there are white solid lumps, and these are thought to be tumors. Some could be seen quite clearly, but some are quite obscure.

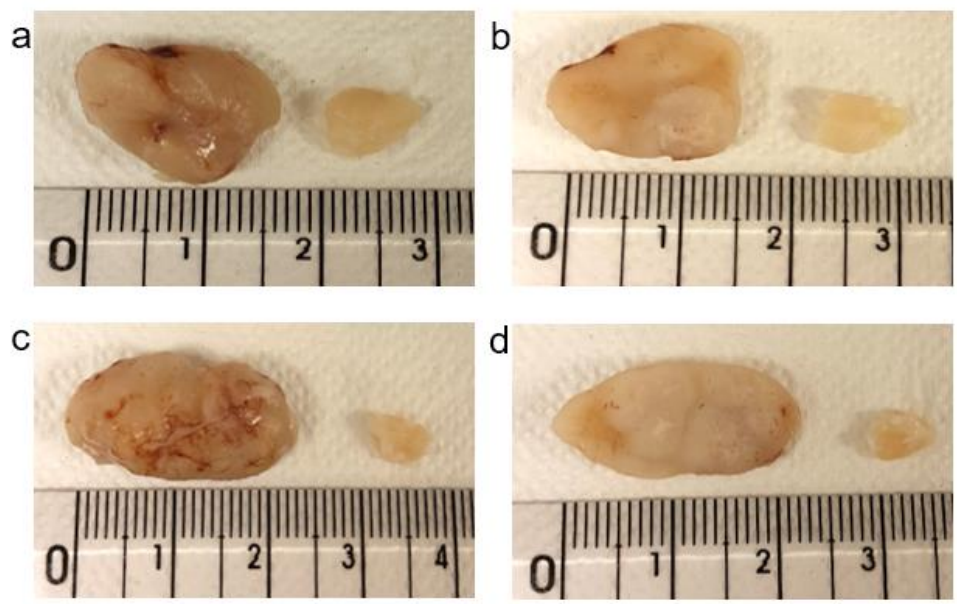

Figure 2. Group A size comparison between the Metastatic and the Normal LN. a) Type 1 before dissection b) Type 1 after dissection c) Type 2 before dissection d) Type 2 after dissection

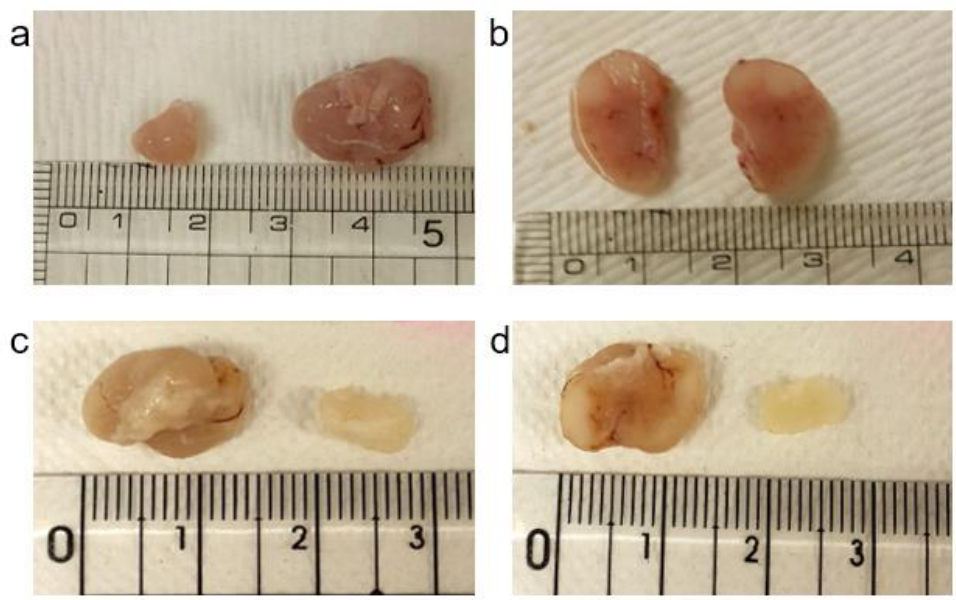

Figure 3. *Group B size comparison between the Metastatic and the Normal LN. a) Type 3 before dissection b) Type 3 after dissection c) Type 4 before dissection d) Type 4 after dissection*

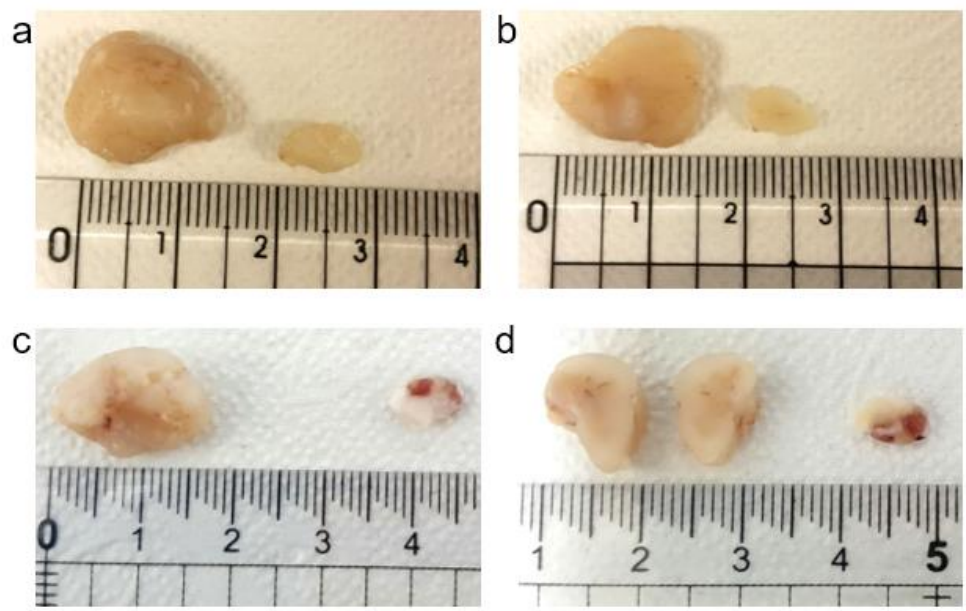

Figure 4. *Group B size comparison between the Metastatic and the Normal LN. a) Type 5 before dissection b) Type 5 after dissection c) Type 6 before dissection d) Type 6 after dissection*

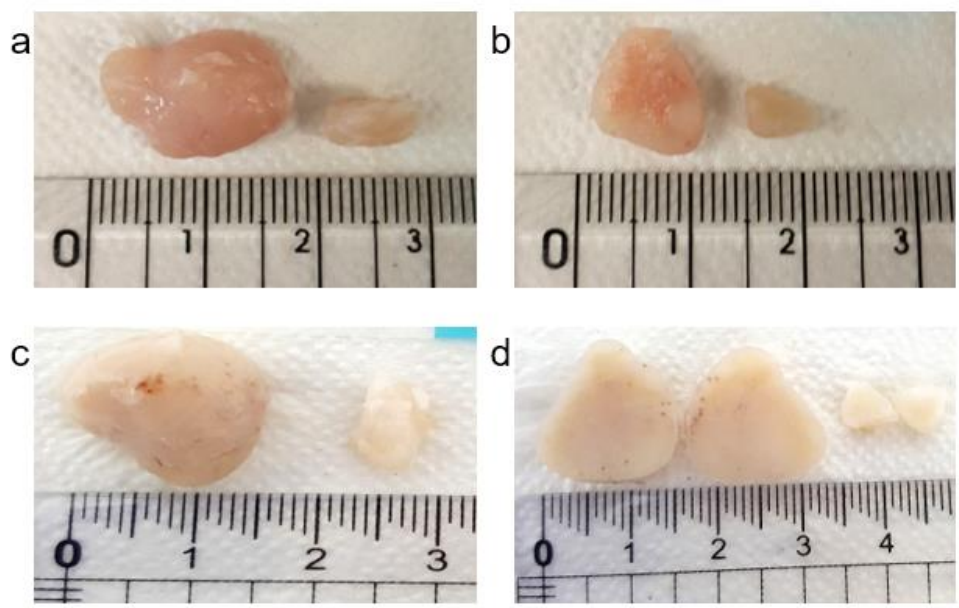

Figure 5. Group C size comparison between the Metastatic and the Normal LN. a) Type 9 before dissection b) Type 9 after dissection c) Type 11 before dissection d) Type 11 after dissection

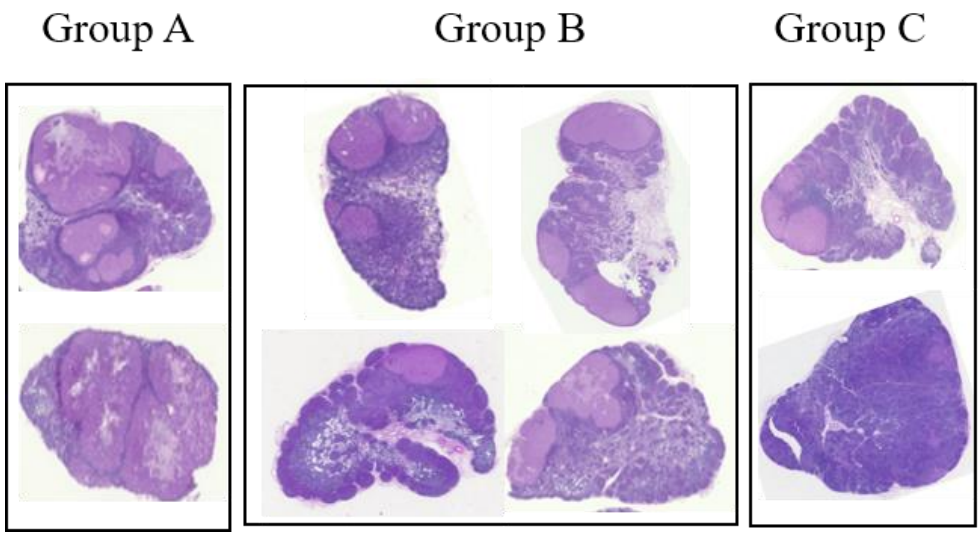

Figure 6. H&E staining showing the appearances of the tumor formations

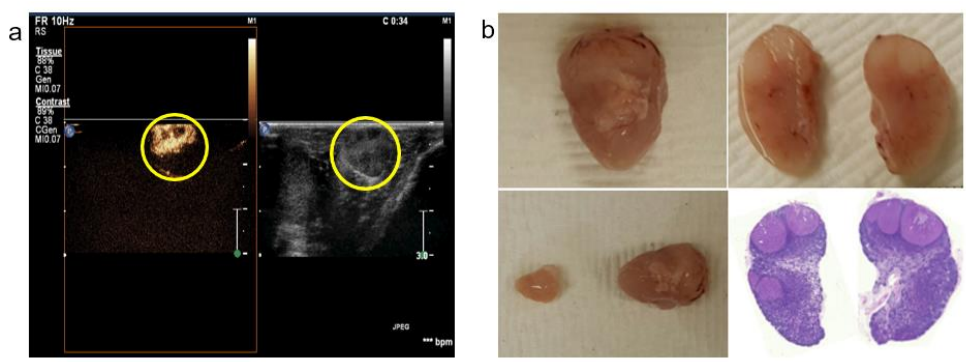

Figure 7. a) VX2 Metastatic lymph node imaging of Rabbit type 3 (Left) SonoVue enhanced imaging, (Right) Grey scale. b) (From top left, clockwise) Metastatic lymph node, Center sliced Metastatic lymph node, H&E staining, size comparison between the normal and the metastatic lymph node

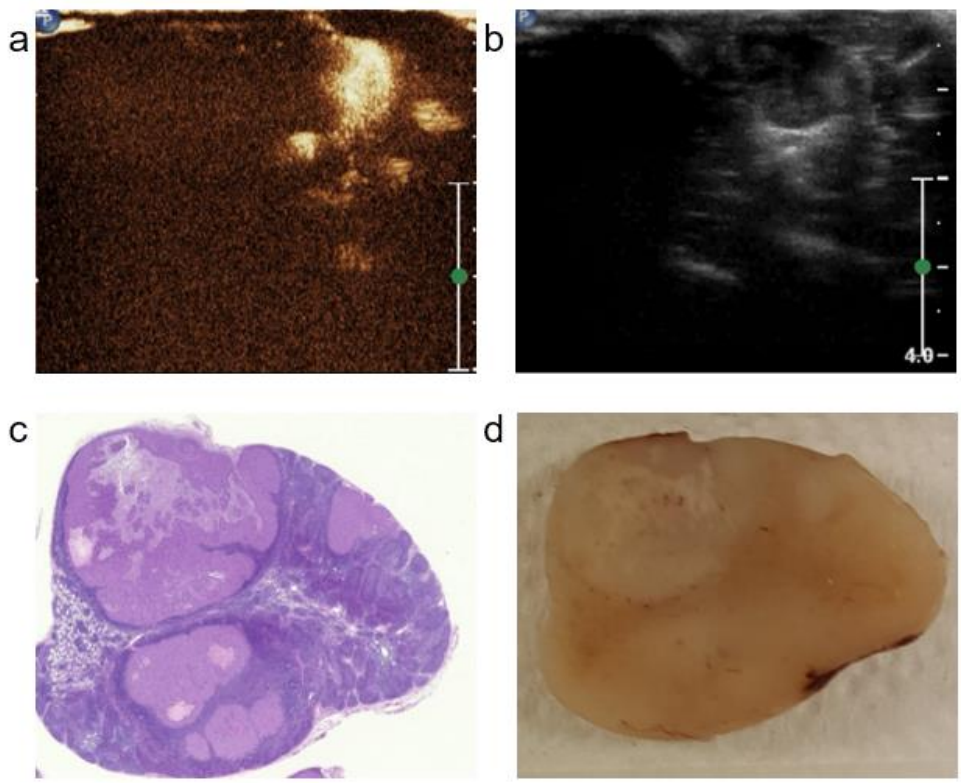

Figure 8. Group A, Type 1 a) SonoVue enhanced ultrasound image, b) grey scale ultrasound image, c) H&E stain, d) tissue image of the metastatic lymph node

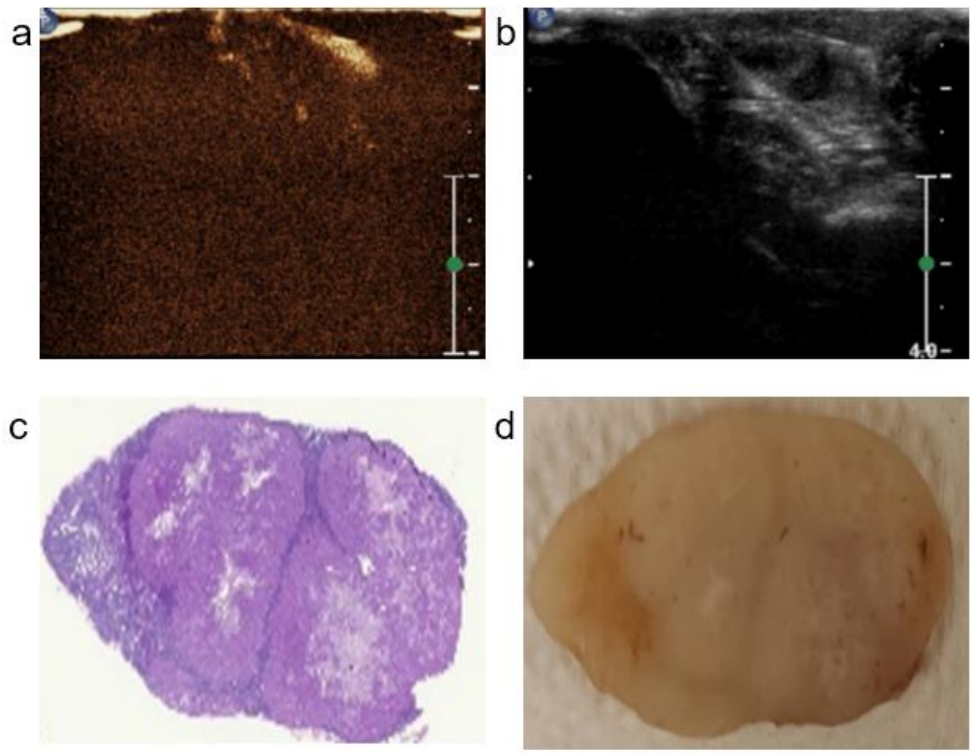

Figure 9. Group A, Type 2 a) SonoVue enhanced ultrasound image, b) grey scale ultrasound image, c) H&E stain, d) tissue image of the metastatic lymph node

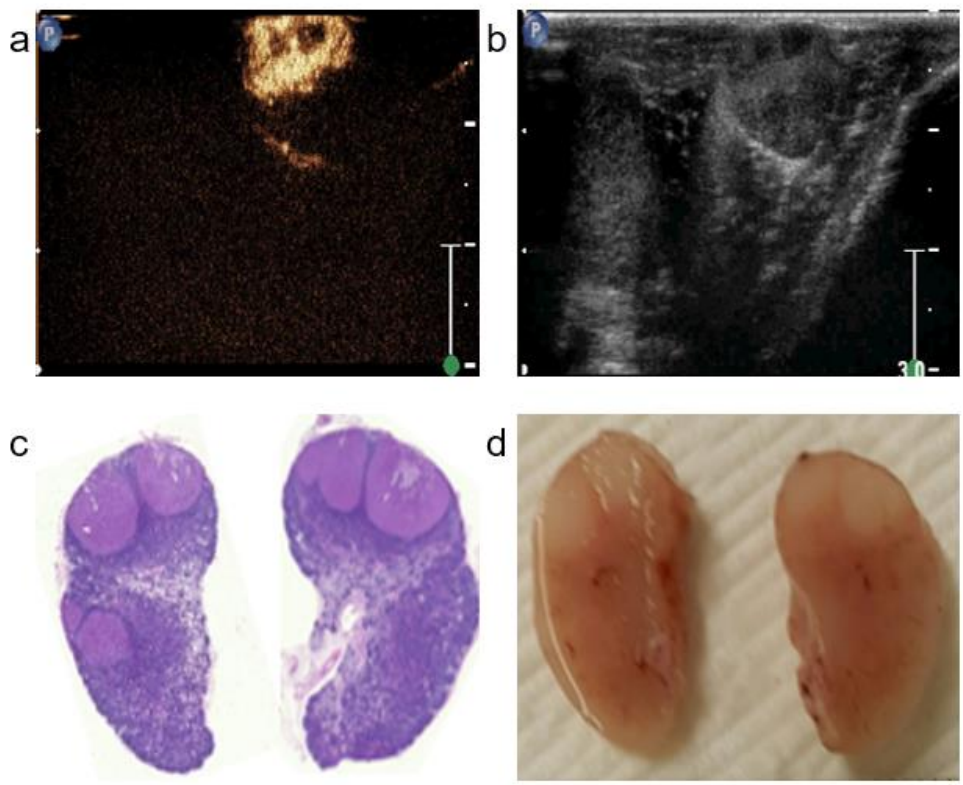

Figure 10. *Group B, Type 3 a) SonoVue enhanced ultrasound image, b) grey scale ultrasound image, c) H&E stain, d) tissue image of the metastatic lymph node*

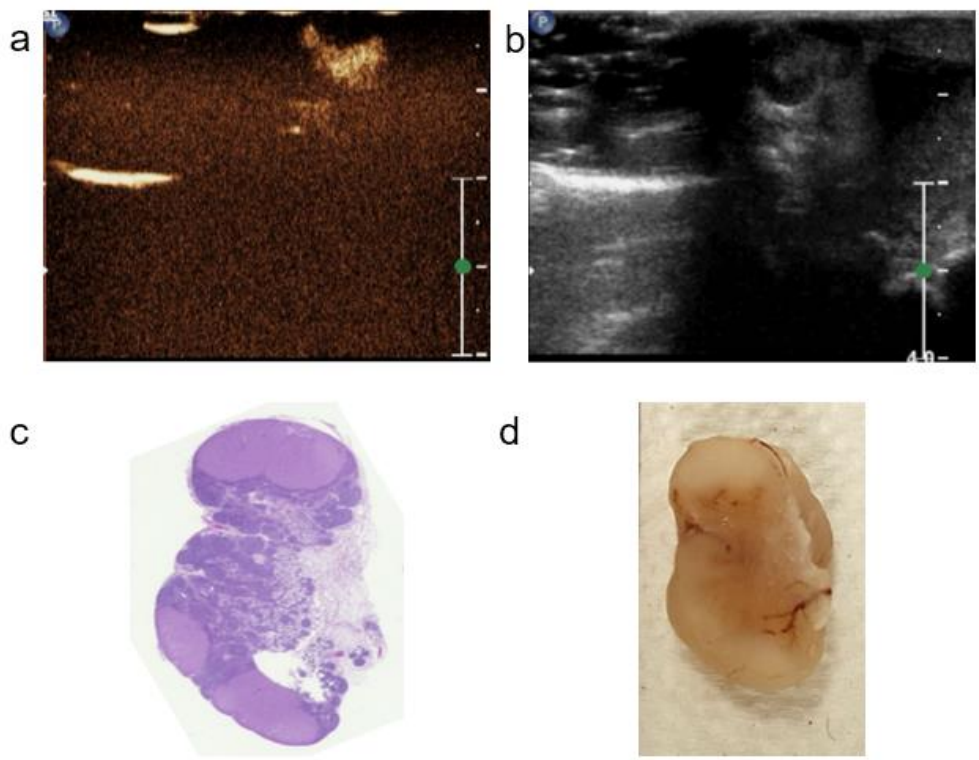

Figure 11. Group B, Type 4 a) SonoVue enhanced ultrasound image, b) grey scale ultrasound image, c) H&E stain, d) tissue image of the metastatic lymph node

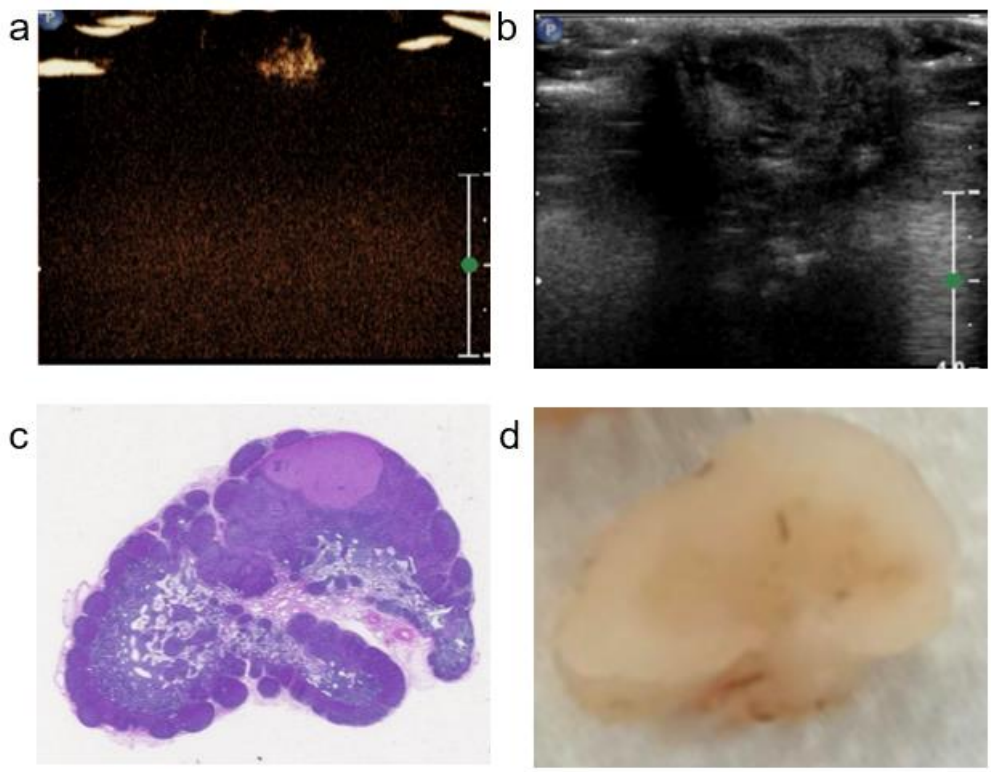

Figure 12. Group B, Type 5 a) SonoVue enhanced ultrasound image, b) grey scale ultrasound image, c) H&E stain, d) tissue image of the metastatic lymph node

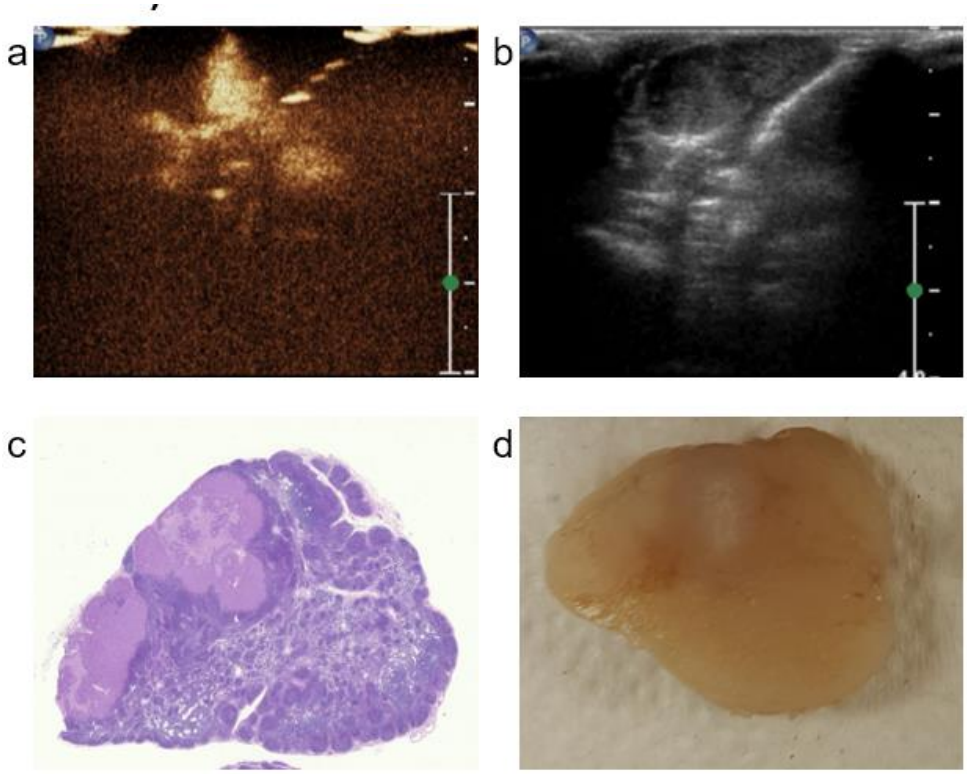

Figure 13. Group B, Type 6 a) SonoVue enhanced ultrasound image, b) grey scale ultrasound image, c) H&E stain, d) tissue image of the metastatic lymph node

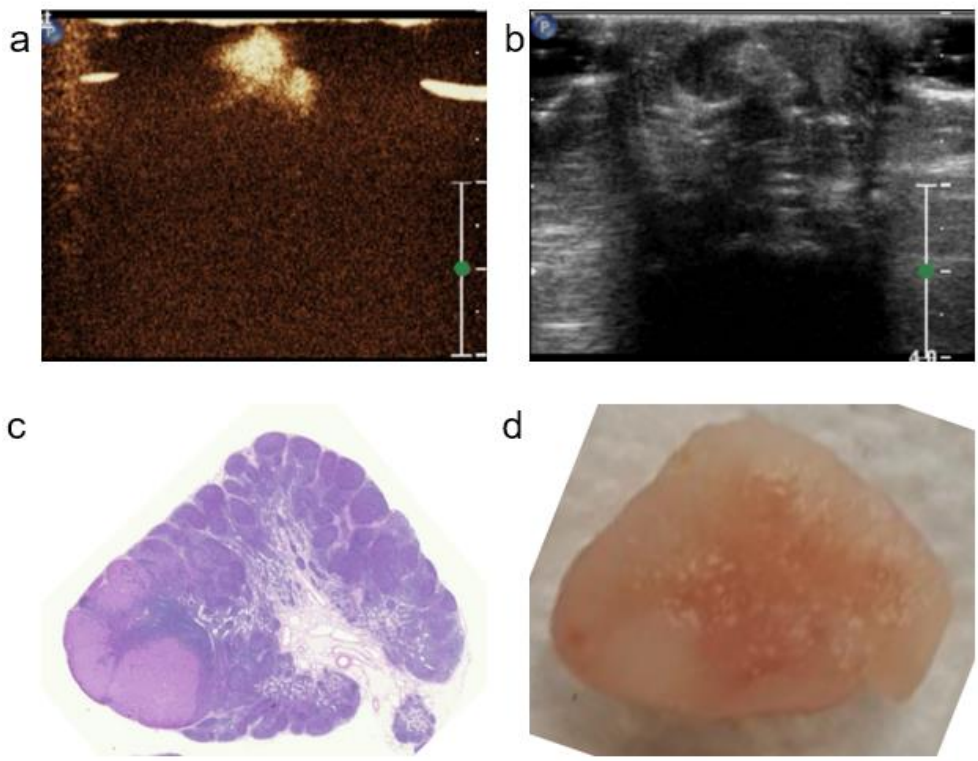

Figure 14. *Group C, Type 9 a) SonoVue enhanced ultrasound image, b) grey scale ultrasound image, c) H&E stain, d) tissue image of the metastatic lymph node*

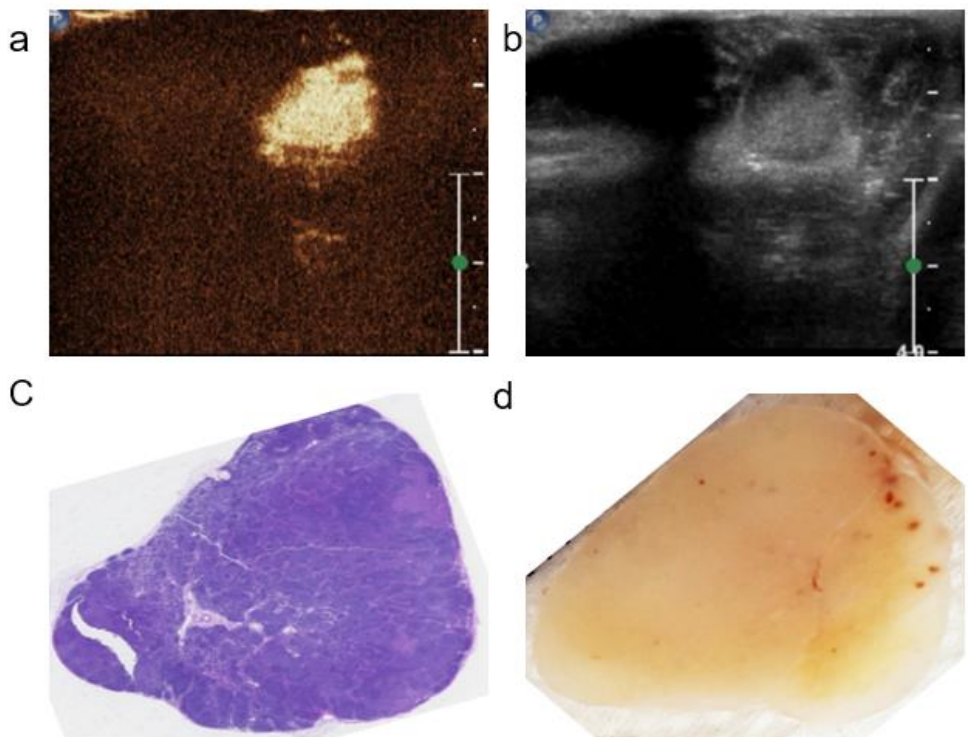

Figure 15. Group C, Type 11 a) SonoVue enhanced ultrasound image, b) grey scale ultrasound image, c) H&E stain, d) tissue image of the metastatic lymph node

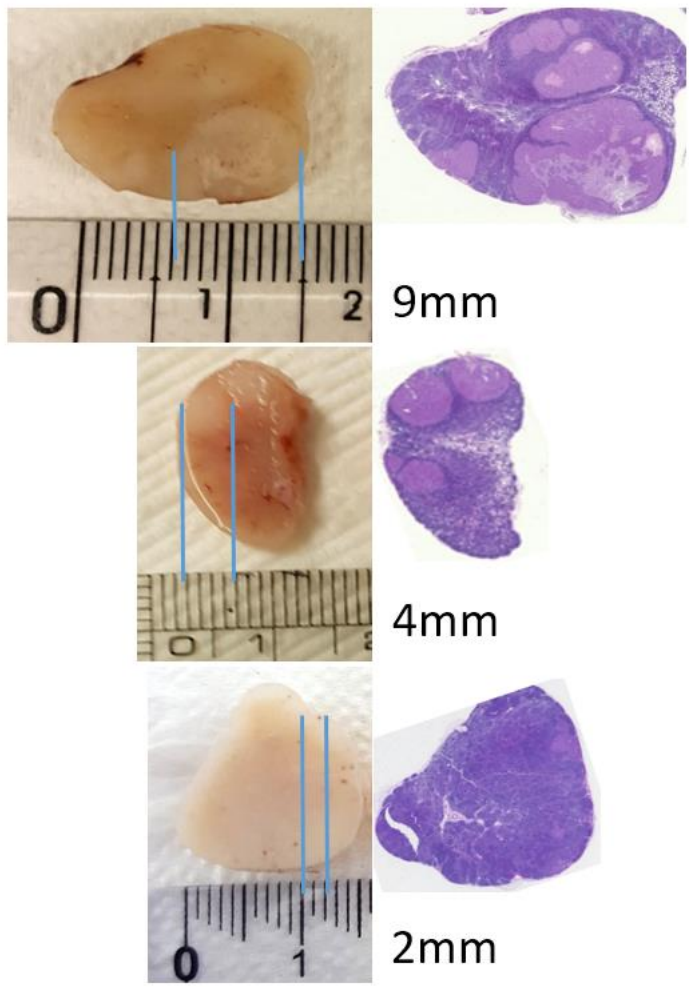

Figure 16. Metastatic lymph nodes from each group.

Top: Group A (Type 1), Middle: Group B (Type 3), Bottom: Group C (Type 11)

5. Discussion

Prior preparing the tumor rabbit models, image acquiring process has been carried out on the normal New Zealand white rabbit to confirm the possibility of spotting the area of interest using the ultrasound scanner (iU22, Philips, Bothell, WA, USA). Utilizing the ultrasound probe (5~12 MHz broadband linear probe), popliteal lymph node on the shaved left hind limb has been spotted and the clear image of lymph node was acquired (Figure 1a). After confirming the presence of popliteal lymph node, SonoVue, a commercially available ultrasound contrast agent, was injected at the bottom of the left foot towards the limb. Ultrasound image of the popliteal lymph node has been acquired after 1 minute of gentle massage on the area of interest (Figure 1b).

Three groups were divided based on the days passed after the subculture process for inducing tumors. Rabbits in Group A were tested 23 days after the VX2 subculture, rabbits in Group B after 19 days, and rabbits in Group C after 14 days. VX2 tumor cell line was only injected in the popliteal lymph node of left hind limb, with the

popliteal lymph node on the right hind limb acting as a control. As seen from the (Table 1), normal LN sizes were quite consistent, in between 0.6~0.9cm with no specific upwards or downwards trends. In the case of metastatic LN, all were observed to be larger than normal LN, in between 1.4~2.5cm, but again with no specific trends. Before the study, positive correlation between the sizes of metastatic LN and the longevity of subculture was assumed. However, although tumor sizes and appearances were distinguishable between each group (Figure 2~Figure 5), sizes of metastatic LN as a whole and the longevity of subcultures did not show any kind of correlations. All were enlarged but no specific trends. All of 11 prepared VX2 tumor rabbit models showed the signs of enlarged lymph nodes compared to the normal lymph nodes, implying that tumors could have been induced in all 11 rabbit models. However, three models, rabbit number 7 in Group B, rabbit number 8 and 10 from the Group C, did not show the signs of tumor, which were confirmed by the dissection pictures as well as the histochemical staining. By percentage, 100 percentage tumor

formations were observed in Group A, in which rabbits had been sub-cultured with the VX2 tumor cells for the most number of days, 80 percentages in Group B, and 50 percentages in Group C, in which rabbits had been sub-cultured for the least number of days. Again, although more rabbits would be needed for more accurate assumptions, days of sub-culture with the tumor cell line seems to have linear positive correlations with the tumor formation rates. The longer the subculture days, the higher the possibilities that tumors would be induced, which means early yet accurate detection of tumor is very important before possible cancer cells spread to other parts of the body via lymphatic systems and cause more serious damages. Histochemical staining images (Figure 6) clearly show the appearances of the induced tumors within the rabbit models. Majorities of metastatic lymph nodes in Group A are infiltrated with the induced tumors, roughly 60~90% by area. For the case of Rabbit 1, two distinctive tumors could be seen (Figure 6, Group A top) and SonoVue enhanced ultrasound imaging confirms the existence of two tumors (Figure 8) since two round dark spots

are imaged next to the brightly spotted area, which matches the area of tumors. Tumors are shown as dark spots since liquid state ultrasound contrast agent cannot infiltrate the solid tumor while viewing in real time. Rabbit 2 (Figure 6, Group A, bottom) had the biggest tumor induction out of all the rabbits tested, with only the area near the surface of the metastatic lymph nodes being intact, and again was confirmed by the SonoVue enhanced ultrasound image which only showed the bright spots on the outside of the popliteal lymph nodes. As in the case with the rabbit 1 and 2 from Group A, appearances of the tumors, such as shapes and sizes, within the metastatic lymph nodes of rabbits in Group B and C were all accurately distinguishable on the acquired ultrasound images (Figure 10~Figure 15). Areas of tumors match the dark spots of the SonoVue enhanced ultrasound images, most notable being the rabbit 3 (Figure 7). (Figure 7a) clearly shows two dark spots within the metastatic lymph node implying two separate tumors, and histochemical stain (Figure 7b, bottom right) confirms the match of the precise area of the tumors.

The smallest tumor formation was observed within the metastatic lymph node of rabbit 11 in Group C, which was around 2mm in length (Figure 16). SonoVue enhanced ultrasound image has shown one dark spot within the brightly imaged SonoVue infiltrated metastatic lymph node, which matches where the tumor is located (Figure 15). (Figure 16) shows one of metastatic lymph nodes from each group, which has been dissected and tumor sizes within the lymph nodes measured. Tumor sizes followed the expected general trend of decreasing down from Group A to Group C, with no tumors found in Group C observed to be bigger than the tumors found in Group B, and again no tumors found in Group B observed to be bigger than the tumors found in Group A. Tumors ranging from 2mm in length to tumors bigger than 9mm within the popliteal lymph nodes were all possible to distinguish via SonoVue enhanced ultrasound imaging modality. However, when tumors are too big in size and the distance between induced tumors are too close (Figure 9), ultrasound image could not accurately distinguish whether there is a one big tumor or multiple tumors close to each other.

6. Bibliography

1. Haffty, B.G., et al., *Locoregional relapse and distant metastasis in conservatively managed triple negative early-stage breast cancer.* Journal of Clinical Oncology, 2006. 24(36): p. 5652-5657.
2. Mariani, G., et al., *Radioguided Sentinel Lymph Node Biopsy in Breast Cancer Surgery*.* Journal of Nuclear Medicine, 2001. 42(8): p. 1198-1215.
3. Galema, T., et al., *Clinical usefulness of SonoVue contrast echocardiography: the Thoraxcentre experience.* Netherlands Heart Journal, 2007. 15(2): p. 55-60.
4. Silberstein, J.L. and V.P. Laudone, *Pelvic lymph node dissection for prostate cancer*, in *Radical Prostatectomy*. 2014, Springer. p. 57-74.
5. Cagiannos, I., et al., *A preoperative nomogram identifying decreased risk of positive pelvic lymph nodes in patients with prostate cancer.* The Journal of urology, 2003. 170(5): p. 1798-1803.
6. Abdollah, F., et al., *National comprehensive cancer network practice guidelines 2011: need for more accurate recommendations for pelvic lymph node dissection in prostate cancer.* The Journal of urology, 2012. 188(2): p.

423-428.

7. Khullar, O.V., et al., *Preclinical Study of Near-Infrared-Guided Sentinel Lymph Node Mapping of the Porcine Lung.* The Annals of thoracic surgery, 2013. 95(1): p. 312-318.

8. Spaliviero, M., et al., *Detection of Lymph Node Metastases with SERRS Nanoparticles.* Molecular Imaging and Biology, 2016: p. 1-9.

9. Godoy, G., et al., *Pelvic lymph node dissection for prostate cancer: frequency and distribution of nodal metastases in a contemporary radical prostatectomy series.* The Journal of urology, 2012. 187(6): p. 2082-2086.

10. Nepple, K.G., et al. *Concordance of preoperative prostate endorectal MRI with subsequent prostatectomy specimen in high-risk prostate cancer patients*. in *Urologic Oncology: Seminars and Original Investigations*. 2013. Elsevier.

11. Meinhardt, W., et al., *Laparoscopic sentinel node dissection for prostate carcinoma: technical and anatomical observations.* BJU international, 2008. 102(6): p. 714-717.

12. van der Poel, H.G., et al., *Intraoperative laparoscopic fluorescence guidance to the sentinel lymph node in prostate cancer patients: clinical proof of concept of an integrated functional imaging approach using a multimodal tracer.*

European urology, 2011. 60(4): p. 826-833.

13. Weissleder, R., et al., *Ultrasmall superparamagnetic iron oxide: an intravenous contrast agent for assessing lymph nodes with MR imaging.* Radiology, 1990. 175(2): p. 494-498.

14. Harisinghani, M.G., et al., *Noninvasive detection of clinically occult lymph-node metastases in prostate cancer.* New England Journal of Medicine, 2003. 348(25): p. 2491-2499.

15. Kircher, M.F. and J.K. Willmann, *Molecular body imaging: MR imaging, CT, and US. Part I. Principles.* Radiology, 2012. 263(3): p. 633-643.

16. Kircher, M.F. and J.K. Willmann, *Molecular body imaging: MR imaging, CT, and US. Part II. Applications.* Radiology, 2012. 264(2): p. 349-368.

17. Schneider, M., *Characteristics of SonoVue™.* Echocardiography, 1999. 16(s1): p. 743-746.

18. Gramiak, R. and P.M. Shah, *Echocardiography of the aortic root.* Investigative radiology, 1968. 3(5): p. 356-366.

19. Claudon, M., et al., *Guidelines and good clinical practice recommendations for contrast enhanced ultrasound (CEUS) - update 2008.* Ultraschall in der Medizin-European Journal of Ultrasound, 2008. 29(01): p. 28-44.

20. Piscaglia, F., et al., *The EFSUMB Guidelines and Recommendations on the Clinical Practice of Contrast Enhanced Ultrasound (CEUS): update 2011 on non-hepatic applications.* Ultraschall in der Medizin-European Journal of Ultrasound, 2012. 33(01): p. 33-59.

21. Tang, M.-X., et al., *Quantitative contrast-enhanced ultrasound imaging: a review of sources of variability.* Interface Focus, 2011. 1(4): p. 520-539.

22. Lassau, N., et al., *Advanced hepatocellular carcinoma: Early evaluation of response to bevacizumab therapy at dynamic contrast-enhanced US with quantification—Preliminary results 1.* Radiology, 2011. 258(1): p. 291-300.

23. Sugimoto, K., et al., *Hepatocellular carcinoma treated with sorafenib: early detection of treatment response and major adverse events by contrast-enhanced US.* Liver International, 2013. 33(4): p. 605-615.

24. Rognin, N.G., et al., *Parametric imaging for characterizing focal liver lesions in contrast-enhanced ultrasound.* IEEE transactions on ultrasonics, ferroelectrics, and frequency control, 2010. 57(11): p. 2503-2511.

25. Rognin, N., et al., *Parametric images based on dynamic behavior over time*. 2015, Google Patents.

26. Tranquart, F., et al., *Perfusion quantification in contrast-enhanced ultrasound (CEUS)-ready for research projects and routine clinical use.* Ultraschall in der Medizin-European Journal of Ultrasound, 2012. 33(S 01): p. S31-S38.

27. Angelelli, P., et al., *Interactive visual analysis of contrast-enhanced ultrasound data based on small neighborhood statistics.* Computers & Graphics, 2011. 35(2): p. 218-226.

28. Bernstein, L.H., *Archive for May, 2013.* PLoS Biol, 2010. 8(1).

29. Anaye, A., et al., *Differentiation of focal liver lesions: usefulness of parametric imaging with contrast-enhanced US.* Radiology, 2011. 261(1): p. 300-310.

30. Yuan, Z., et al., *Diagnostic value of contrast-enhanced ultrasound parametric imaging in breast tumors.* Journal of breast cancer, 2013. 16(2): p. 208-213.

31. Lindner, J.R., *Microbubbles in medical imaging: current applications and future directions.* Nature Reviews Drug Discovery, 2004. 3(6): p. 527-533.

32. McCulloch, M., et al., *Ultrasound contrast physics: a series on contrast echocardiography, article 3.* Journal of the American Society of Echocardiography, 2000. 13(10): p. 959-967.

7. Abstract in Korean

초음파 조영제를 이용한 토끼 종양의 전이 림프절 평가에 관한 연구

이 현 재
융합과학부 나노융합학과
서울대학교 융합과학기술대학원

이 연구는 복잡한 전이성 토끼 종양 모델 확립을 위해 진행되었습니다. 초음파 조영제가 토끼 종양 모델의 전이성 림프절 내에서 어떤 식으로 영상이 보이는지, 사용한 조영제를 사용해 얼마나 작은, 또는 큰 종양을 정확하게 영상으로 보고 분별할 수 있는지 등을 중점적으로 연구하였습니다. 11 마리 의 토끼 종양 모델을 사용하였고, 계대배양 날짜에 따라서 세 그룹으로 나누었습니다. 정상 림프절 사이즈는 모든 그룹에서 비슷하고, 전이성 림프절도 모든 그룹에서 비슷한 사이즈였지만, 전이성 림프절은 정상 림프절과 비교해서 확연히 커져있는 걸 확인할 수 있었습니다. 전이성 림프절들의 사이즈는 비슷했지만 그 속에 생성된 종양 모양은 모든 림프절마다 다르게 보였고, 초음파 조영제를 투여했을 때, 종양, 특히 부분적으로만 생성된 작은

종양도 어디에 있는지 정확한 위치를 초음파 영상에서 확인할 수 있는 가능성을 보았습니다. 다음엔 확립된 전이성 토끼 종양 모델을 바탕으로 나노 크기의 조영제 등을 사용한 다양한 초음파 실험과 병리학적 비교 소견 연구 등을 진행해볼 계획입니다.

주요어 : 초음파 조영제, 전이성 림프절, 토끼, 종양
학 번 : 2014-24881